DOI: 10.11776/j.issn.1000-4939.2025.03.020

TAN Saifei^1^, WANG Xuanzhi^1^, ZHANG Meiling^1^, LIU Changgen^1^, WANG Aimin^2^, XU Xiaofu^3^, XU Peng^4^

2025-06-25

ChinaRxiv

Abstract

Rectangular frame-type artificial reefs can be employed to modify flow fields, providing favorable habitats for various marine organisms. In tropical marine areas such as the offshore waters of Hainan Island, they can also serve as attachment substrates for coral restoration. Flow velocities at representative measurement points of rectangular frame-type artificial reef models were measured using an acoustic Doppler velocimeter (ADV), and typical flow field characteristics around the reef models were further measured using particle image velocimetry (PIV). Based on the RANS equations and RNG k-ϵ turbulence model, the hydrodynamic field of a single rectangular frame-type artificial reef under different incoming flow velocities and flow incidence angles was numerically calculated and validated through experiments. On this basis, the flow field effects of multiple reefs under different deployment configurations were computed and analyzed. The results demonstrate that: within a certain range, the upwelling and wake vortex volumes of a single reef increase with increasing incoming flow velocity, and the flow field effect is optimal when deployed at a flow incidence angle of 45°; the flow field effect is optimal when the reef deployment spacing is 2.5 times the reef length in the longitudinal direction and 1.5 times the reef length in the transverse direction; when reef groups composed of multiple reefs are deployed linearly, staggered front-to-back arrangement of reef rows yields larger upwelling and wake vortex volumes, resulting in superior flow field effects.

Full Text

DOI: 10.11776/j.issn.1000-4939.2025.03.020

Flow-Field Effects of Cuboid Frame-Type Artificial Reefs

TAN Saifei[1], WANG Xuanzhi[1], ZHANG Meiling[1], LIU Changgen[1], WANG Aimin[2], XU Xiaofu[3], XU Peng[4]

(1. Department of Mechanics, School of Mechanical Engineering, Tianjin University, 300350 Tianjin; 2. College of Oceanography, Hainan University, 570228 Haikou;
3. Tianjin Fisheries Research Institute, 300457 Tianjin; 4. College of Marine Ecology and Environment, Shanghai Ocean University, 201306 Shanghai)

Abstract: Cuboid frame-type artificial reefs can be used to alter the flow field and provide favorable habitat environments for various marine organisms; in tropical waters such as the offshore waters of Hainan Island, they can also provide attachment substrates for coral restoration. An acoustic Doppler velocimeter (ADV) was used to measure the flow velocity at representative measuring points of a cuboid frame-type artificial reef model, and particle image velocimetry (PIV) was further used to measure typical flow-field characteristics around the reef model. Based on the RANS equations and the RNG $k-\varepsilon$ turbulence model, the hydrodynamic field of a single cuboid frame-type artificial reef under different incoming-flow velocities and incident-flow angles was numerically calculated, and the results were verified using the experiments. On this basis, the flow-field effects of multiple reef bodies under different deployment arrangements were calculated and analyzed. The results show that, within a certain range, the volumes of the upwelling region and back-vortex region of a single reef body increase with increasing incoming-flow velocity; when the incident-flow angle is 45°, the flow-field effect is optimal. The flow-field effect is optimal when reefs are deployed with a longitudinal spacing of 2.5 times the reef length and a transverse spacing of 1.5 times the reef length. For reef groups composed of multiple reef bodies arranged in a straight-line layout, a staggered front-rear arrangement of the reef bodies in each row produces larger upwelling and back-vortex volumes and yields better flow-field effects.

Keywords: artificial reef; flow-field effect; upwelling and back vortex; deployment spacing; optimized layout

Chinese Library Classification No.: S953.1 **Document Code:** A **Article No.:** 1000-4939(2025)03-0665-12

Flow field effect of cuboid frame artificial reef

TAN Saifei[1], WANG Xuanzhi[1], ZHANG Meiling[1], LIU Changgen[1], WANG Aimin[2], XU Xiaofu[3], XU Peng[4]

(1. Department of Mechanics, School of Mechanical Engineering, Tianjin University, 300350 Tianjin, China;
2. College of Oceanography, Hainan University, 570228 Haikou, China; 3. Tianjin Bohai Sea Fisherise Research Institute, 300457 Tianjin, China; 4. College of Marine Ecology and Environment, Shanghai Ocean University, 201306 Shanghai, China)

Abstract: The cuboid frame artificial reefs can be used to change the flow field and provide a favorable habitat for a variety of marine life. In tropical waters such as offshore Hainan Island, artificial reefs can also provide an attachment base for coral restoration. In this paper, ADV was used to measure the flow velocity of the representative measuring points of the cuboid frame artificial reef model, and PIV was further used to measure the typical flow field characteristics around the reef model. Based on RANS equations and RNG $k-\varepsilon$ turbulence model, the hydrodynamic field of a single cuboid frame artificial reef was numerically cal-

---

Date received: 2022-10-03
Fund projects: National Key R&D Program of China (No. 2018YFD0900704);

National Natural Science Foundation of China (No. 42016002); Tianjin Municipal Science and Technology Major Special Project and Engineering Funding Project (No. 18ZXRHSF00270); Tianjin University-Hainan University Independent Innovation Fund Project (No. 2020XZC-0097)

Corresponding author: LIU Changgen, Associate Professor. E-mail: lchg@tju.edu.cn

Citation format: TAN Saifei, WANG Xuanzhi, ZHANG Meiling, et al. Flow-field effects of cuboid frame-type artificial reefs[J]. Chinese Journal of Applied Mechanics, 2025, 42(3): 665–676.
TAN Saifei, WANG Xuanzhi, ZHANG Meiling, et al. Flow field effect of cuboid frame artificial reef[J]. Chinese journal of applied mechanics, 2025, 42(3): 665–676.

culated under different incoming flow velocities and angles of incident flow, which was verified by experimental results. On this basis, the flow field effects of multiple reefs under different layout modes were calculated and analyzed. The results show that within a certain range, the volume of upwelling and back eddy of a single reef increases as the velocity of incoming stream increases, and the flow field effect is best when the angle of incident flow is 45°. The best field effect of two reefs is obtained at the spacing of 2.5 times of the length of the longitudinal reef and 1.5 times of the length of the transverse reef. When multiple reefs are arranged along a straight line, the staggered arrangement of each row of reefs has a larger volume of upwelling and back eddy, and the flow field effect is better.

Key words: artificial reef; flow field effect; upwelling and back eddy; layout spacing; optimized layout

Artificial reefs are man-made structures placed in natural marine environments. Reef bodies of various shapes form reef groups through different arrangement methods; they are used to restore aquatic ecosystems and provide breeding, growth, and habitat sites for various marine organisms. In tropical marine ranches such as those around Hainan Island, artificial reefs are also widely distributed as an attached substrate for coral restoration. Under the action of tidal currents, bottom sediments and nutrient salts are lifted by the upwelling generated on the upstream face of artificial reefs, increasing the repeated use of deposited bait within the area and benefiting the aggregation of fish. At the same time, because the tidal current is affected by the artificial reef, the flow velocity in the region behind the reef body decreases, forming a large-volume vortex, which is therefore called the back-eddy flow region. A relatively large back-eddy region can provide breeding and resting places for fish[^1]. Therefore, upwelling and back-eddy flow are important bases for studying the flow-field effects of artificial reefs.

Research on the hydrodynamics of artificial reefs mainly includes model experiments[^2-8] and numerical simulation experiments[^8-14], both of which have achieved certain results. Liu Yan et al.[^15] used particle image velocimetry (PIV) to study the flow field of single and double combined star-shaped artificial reefs at different flow velocities. Mo Congda et al.[^16] used numerical simulation to study the scale of upwelling and back-eddy flow formed by artificial ship reefs of different sizes under different combination modes, and established an optimal deployment mode for artificial ship reefs. Liu Hongsheng et al.[^17] studied the flow fields of cube, pyramid, and three-prism artificial reef models through wind-tunnel experiments. LIU et al.[^18] used numerical simulation to study the influence of changes in reef-body layout on the surrounding flow field of square porous artificial reefs, and provided suggestions for the layout method of two reef bodies. LIU et al.[^19] designed a three-dimensional numerical model to calculate the unsteady flow field around star-shaped artificial reefs and discussed the influence of layout spacing on the flow fields of single and double artificial reefs. LAN et al.[^20-21], comprehensively considering such factors as reef-group budget, reef-body cost, reef-body spacing, and the number of reef bodies, proposed a reef-group layout model (LARCs) and a deployment model (DARCs), providing a basis for the layout of unit reefs. WANG et al.[^22] studied the influence of opening ratio (OR), opening shape (OS), and opening number (ON) on the flow field of cubic artificial reefs, providing a reference for the structural design of cubic artificial reefs. Jiang Zhaoyang et al.[^23] used model experiments and numerical simulations to study the hydrodynamic and flow-field characteristics of artificial reef models in constant flow. Li Qiao et al.[^24] studied the intensity and scale of the flow-field effects around tubular artificial reefs by comparing particle image velocimetry experiments with numerical simulations. The above scholars analyzed the flow-field effects of reefs of different shapes under different flow velocities, different opening ratios, and different incident-flow angles by using different research methods.

When the number of artificial reefs is large, the relationship between the arrangement method and the flow-field effect is relatively complex. At present, there are still few studies on the flow-field effects and arrangement methods of relatively large-scale artificial reef groups. In terms of quantitative analytical methods for evaluating flow-field effects, compared with the traditional evaluation methods of measuring upwelling height and back-eddy length[^25] and analyzing the two-dimensional areas of upwelling and back-eddy flow[^26], the use of three-dimensional integration to calculate the volumes of upwelling and back-eddy flow can yield more accurate results[^27]. Rectangular frame-type artificial reefs are easy to stack and convenient to transport and deploy. Their structure is simple, and a cage structure can extend upward from them, facilitating attachment by marine organisms such as oysters and corals. They are an excellent substrate for coral restoration and a reef type relatively suitable for coral restoration. At present, they have been used for ecological restoration in tropical marine ranches around Hainan Island, and have also been used for artificial restoration of corals, achieving good results. Acoustic Doppler velocimeter (ADV) velocity-measurement experiments can measure the instantaneous flow velocity at a single point; by using multiple ADVs or moving the ADV position, verification of measurement points over a larger area can be performed. PIV particle-velocity-measurement experiments can obtain instantaneous velocities over the entire field, but the field of view is relatively small[^28], so only local flow-field structural information can be obtained. In this work, an ADV was used to measure the flow velocities at typical measurement points of a rectangular frame-type artificial reef model, and PIV was further used to measure the flow-field characteristics around the reef model. Based on the RANS equations and the RNG $k-\varepsilon$ turbulence model, the hydrodynamic field of a single artificial reef under different incoming flow velocities and angles of incidence was numerically calculated; the results were verified using model experiments. On this basis, the flow-field effects of reef bodies under different deployment spacings and reef groups under different arrangement modes were calculated and analyzed. By calculating the volumes of the upwelling and back-eddy regions, the effects of incoming flow velocity, incident-flow angle, layout spacing, and arrangement mode on the flow-field effects were quantitatively analyzed, with the aim of providing a reference for the deployment of artificial reefs and the optimization of reef-group layouts.

1 Model Experiment

The dimensions of the rectangular frame-type artificial reef are $2\ \mathrm{m} \times 1\ \mathrm{m} \times 1\ \mathrm{m}$ ($L \times W \times H$). The cross section of the bottom crossbeams and columns is $0.2\ \mathrm{m} \times 0.2\ \mathrm{m}$, and the cross section of the top crossbeams is $0.2\ \mathrm{m} \times 0.15\ \mathrm{m}$. Figure 1 is a schematic diagram of the reef model.

Fig. 1 Schematic diagram of artificial reef model (unit: cm)

Figure 1: Fig. 1 Schematic diagram of artificial reef model (unit: cm)

Fig. 1 Schematic diagram of artificial reef model (unit: cm)

PIV experiments and ADV velocity-measurement experiments were carried out in a circulating flume using a scaled artificial reef model. The model scale was $1:10$, and the model was made of organic glass.

The schematic diagram of the experimental setup is shown in Fig. 2. The flume dimensions were $15.0\ \mathrm{m} \times 1.0\ \mathrm{m} \times 1.3\ \mathrm{m}$, and the experimental water depth was 1.0 m. To prevent sliding or rolling of the reef, the reef body was fixed at the central position of the test section of the flume, placed parallel to the incoming-flow direction. The center of the reef bottom was taken as the origin of the coordinate system; the X-axis direction was the flow direction, the Y-axis direction was the water-depth direction, and the Z-axis direction was transverse to the flume, as shown in Fig. 2.

Fig. 2 Schematic diagram of flume experiment device

Figure 2: Fig. 2 Schematic diagram of flume experiment device

Fig. 2 Schematic diagram of flume experiment device

Fig. 3 ADV measuring point layout

Figure 3: Fig. 3 ADV measuring point layout

Fig. 3 ADV measuring point layout

ADV velocity-measurement experiments were carried out above the reef body. The constant incoming-flow velocity was 0.22 m/s. The velocities at measuring points A1–A13 shown in Fig. 3 were measured separately. All measuring points were located on the $Z = 0$ section, 20 cm above the bottom of the flume.

After the ADV measurements were completed, in order to obtain better particle-visualization effects and flow-field information under different flow velocities, and to provide more experimental data for model validation, the flume velocity was reduced to 0.145 m/s. After the flow velocity became stable, PIV experiments were conducted. A CCD high-speed camera was used to shoot from the side of the flume, and the instantaneous velocity fields of the four sections a, b, c, and d shown in Fig. 4 were measured. Sections a and b were imaging fields of view at the middle positions of the reef openings, while sections c and d were imaging fields of view at the middle positions of the reef body. The model experiment results are shown in Fig. 7(a)–Fig. 7(d).

Fig. 4 Schematic diagram of PIV measurement section in model experiment

Figure 4: Fig. 4 Schematic diagram of PIV measurement section in model experiment

Fig. 4 Schematic diagram of PIV measurement section in model experiment

2 Mathematical Model

2.1 Governing Equations and Turbulence Model

The water body is regarded as an incompressible viscous Newtonian fluid. The three-dimensional Reynolds-averaged Navier-Stokes (RANS) equations[^29] are adopted, and the governing equations are as follows.

Continuity equation

$$\frac{\partial u_i}{\partial x_i} = 0 \tag{1}$$

Momentum equation

$$\frac{\partial u_i}{\partial t} + u_j \frac{\partial u_i}{\partial x_j} = f_i - \frac{1}{\rho}\frac{\partial p}{\partial x_i} + \frac{\partial}{\partial x_j}\left(\nu \frac{\partial u_i}{\partial x_j} - \overline{u_i' u_j'}\right) \tag{2}$$

where u_i $(i = 1, 2, 3)$ are the Reynolds-averaged velocities in the x, y, and z directions, respectively; f_i is the body force; p is pressure; ν is the kinematic viscosity coefficient; and ρ is the fluid density.

The Reynolds stress $-\rho\overline{u_i' u_j'}$ is

$$-\rho\overline{u_i' u_j'} = \mu_t \left(\frac{\partial u_i}{\partial x_j} + \frac{\partial u_j}{\partial x_i} \right) - \frac{2}{3} \times \left(\rho k + \mu_t \frac{\partial u_k}{\partial x_k} \right) \delta_{ij} \tag{3}$$

where μ_t is the turbulent viscosity; δ_{ij} is the Kronecker symbol ($i = j,\ \delta_{ij} = 1;\ i \neq j,\ \delta_{ij} = 0$).

The RNG $k-\varepsilon$ turbulence model is relatively suitable for numerical simulation of the flow field around artificial reefs[^30].

The turbulent kinetic energy k equation is

$$\frac{\partial(\rho k)}{\partial t} + \frac{\partial(\rho k u_i)}{\partial x_i} = \frac{\partial}{\partial x_j} \left(\alpha_k \mu_{\text{eff}} \frac{\partial k}{\partial x_j} \right) + G_k - \rho\varepsilon \tag{4}$$

The turbulent dissipation rate ε equation is

$$\frac{\partial(\rho\varepsilon)}{\partial t} + \frac{\partial(\rho\varepsilon u_i)}{\partial x_i} = C^*_{1\varepsilon} \frac{\varepsilon}{k} G_k - C_{2\varepsilon} \rho \frac{\varepsilon^2}{k} + \frac{\partial}{\partial x_i} \left(\alpha_\varepsilon \mu_{\text{eff}} \frac{\partial \varepsilon}{\partial x_j} \right) \tag{5}$$

where G_k is the increase in turbulent kinetic energy caused by the mean velocity gradient; μ_{eff} is the effective turbulent viscosity coefficient; α_k and α_ε are the reciprocals of the effective turbulent Prandtl numbers for the k and ε equations, respectively; and $C^*_{1\varepsilon}$ and $C_{2\varepsilon}$ are empirical constants. The calculation formulas for these coefficients are expressed as

$$G_k = \mu_t \left(\frac{\partial u_i}{\partial x_j} + \frac{\partial u_j}{\partial x_i} \right) \frac{\partial u_i}{\partial x_j}, \quad \mu_{\text{eff}} = \mu + \mu_t, \quad \mu_t = \rho C_\mu$$

$$\frac{k^2}{\varepsilon}, \quad C_\mu = 0.084\,5, \quad C^*_{1\varepsilon} = 1.42, \quad C_{2\varepsilon} = 1.68, \quad \alpha_k =$$

$$\alpha_\varepsilon = 1.390.$$

2.2 Computational Domain and Boundary Conditions

When numerically simulating a reef body, in order to correctly reflect the flow-field conditions around the artificial reef, the length of the computational domain should reach 9 times the reef length (3 times in front of the reef and 5 times behind the reef), the width of the computational domain should reach 5-6 times the reef width, and the height of the computational domain should reach more than 4 times the reef height[^31]. Therefore, the computational domain is selected as a rectangular parallelepiped with dimensions $12.5L \times 10.0W \times 5.0H$, in which the length of the computational domain in front of the reef is $3.5L$, and the length behind the reef is $8L$, as shown in Fig. 5. Whether for the prototype or the model, the multiples of the computational domain relative to the dimensions of the artificial reef are consistent; therefore, only the relationship between the computational domain and the artificial reef in terms of multiples is given here. The dashed-line portion is the mesh refinement region, with a size of $4L \times 6W \times 3H$. Multiple mesh-independence tests were performed on the computational mesh; the mesh sizes in the refined part of the computational domain were 0.04, 0.05, 0.1, and 0.15 m, respectively. All were tetrahedral meshes, and ten boundary layers were set on the reef surface. The incoming flow velocity was 0.5 m/s. The grid-convergence error was obtained by comparing the volumes of the upwelling flow and wake flow calculated under different mesh sizes with the results from smaller meshes[^32], as shown in Table 1. To ensure computational accuracy and computational efficiency, the computational model in this study selects a mesh size of 0.05 m in the refined region; the maximum mesh size in the computational domain is 0.4 m, and the total number of mesh elements exceeds 5.57 million. In the experimentally validated model, the minimum mesh size is 0.005 m to achieve the same mesh quantity. The computed results provide good resolution of the flow field around the reef.

Fig. 5 Schematic diagram of calculation area of artificial reef model (unit: m)

Figure 5: Fig. 5 Schematic diagram of calculation area of artificial reef model (unit: m)

图 5　人工鱼礁模型计算区域示意图（单位：m）

Fig. 5　Schematic diagram of calculation area of artificial reef model (unit: m)

表 1　网格无关性检验

Tab. 1　Grid independence testing

Minimum mesh size / m	Upwelling-flow region volume / m^3	Grid-convergence error / %	Wake-flow region volume / m^3	Grid-convergence error / %
0.04	177.90	-	142.67	-
0.05	173.26	2.61	133.63	6.34
0.1	141.39	18.39	108.35	18.92
0.15	114.37	19.11	91.73	15.34

The initial boundary conditions for the calculation were as follows: the inlet boundary adopted a velocity-inlet condition; the outlet boundary adopted a free outflow condition; the two lateral sides of the computational domain were set as symmetry boundaries; the top was set as a movable wall surface with the same velocity as the inlet flow velocity; and the bottom and reef-body surfaces were set as no-slip walls[1].

The numerical simulation was based on Fluent software. Pressure–velocity coupling adopted the SIMPLEC algorithm, the momentum equations used a second-order upwind scheme for discretization of the convection terms, and the residual value for the continuity equation was taken as 10^{-5}.

2.3 Model experimental results and validation of the mathematical model

To verify the accuracy of the parameter settings and grid division of the numerical model, the velocity values at 13 measuring points in the ADV velocity-measurement experiment were selected, as shown in Fig. 6. The horizontal axis is the ratio of the measuring-point coordinate X to the reef length L, and the vertical axis is the ratio of the measuring-point flow velocity V to the incoming-flow velocity V_0. Because the measuring points were located where the disturbance from vortical flow near the reef wall was relatively small, the relative error between the calculated and experimental values varied within the range of 0.09%–0.53%, indicating very good agreement. Meanwhile, the flow field in the near region in front of and behind the reef was validated through the PIV experiment; the validation results are shown in Fig. 7. The water-flow velocity in front of the reef decreased because of the resistance generated by the reef body, while the flow velocity in the flow field above the reef increased. In the region behind the reef-body model, the flow velocity decreased slowly and vortices formed. Overall, the velocity distribution of the flow field around the fish-reef model obtained from the experiment and the simulation agreed well.

Fig. 6 Comparison between the calculated and experimental results of ADV measuring point velocity

Figure 6: Fig. 6 Comparison between the calculated and experimental results of ADV measuring point velocity

Fig. 6 Comparison between the calculated and experimental results of ADV measuring point velocity

Fig. 7 Comparison between PIV experiment and calculated flow field velocity vector

Figure 7: Fig. 7 Comparison between PIV experiment and calculated flow field velocity vector

(a) Section a (b) Section b (c) Section c (d) Section d

[1] Reference [33].

Fig. 7 Comparison between PIV experiment and calculated flow field velocity vector

3 Results and Analysis

3.1 Influence of Incoming Flow Velocity and Angle of Attack

The tidal current velocity in the sea area where artificial reefs are deployed varies periodically between 0.09 and 0.49 m/s. It is a reciprocating flow. Taking the direction of the main tidal current as the incoming-flow direction, the placement of a single reef was studied under three angles of attack—0°, 45°, and 90°—as shown in Fig. 8; that is, the reef was placed perpendicular to the main-flow direction, at an oblique angle of 45° to the main-flow direction, and parallel to the main-flow direction. In the numerical simulations, characteristic velocities of $V = 0.1$, 0.3, and 0.5 m/s were taken as the incoming-flow velocities.

Fig. 8 Schematic diagram of individual reef arrangement

Figure 8: Fig. 8 Schematic diagram of individual reef arrangement

Fig. 8 Schematic diagram of individual reef arrangement

Figures 9, 10, and 11 show the flow fields on different sections under three angles of attack at incoming-flow velocities of 0.1, 0.3, and 0.5 m/s, respectively. In each figure, (a) is the velocity contour on the horizontal section $Y = 0.5$ m, and (b) is the velocity vector plot on the vertical section $Z = 0$ m. From Fig. 9(a), Fig. 10(a), and Fig. 11(a), it can be seen that a disturbed low-velocity recirculation zone forms behind each column. When the angle of attack is 45°, owing to the larger projected area facing the flow, a larger deceleration zone is generated in front of the reef body. As the incoming-flow velocity increases, the wake region produced by the reef body also becomes larger. When the angle of attack is 0° or 90°, because of the symmetry of the reef body, the wake generated is also relatively symmetric and contracts toward the center as the flow velocity increases. By contrast, when the reef is placed at 45°, the wake region continuously expands toward both sides as the flow velocity increases, and the area on one side is significantly larger than that on the other. In Fig. 9(b), Fig. 10(b), and Fig. 11(b), a large back-vortex region forms behind the columns. In the space inside the reef body where no columns block the flow, the fluid passes through rapidly, forming a high-speed "middle channel." When the angle of attack is 45°, the space inside the reef body without column obstruction is reduced, and the resulting internal high-speed region is the smallest, giving a better flow-field effect.

(a) Velocity contour of the $Y = 0.5$ m section

(b) Velocity vector image of the $Z = 0$ m section

Fig. 9 Velocity contour of the $Y = 0.5$ m section and velocity vector image of the $Z = 0$ m section under three placement modes when $V = 0.1$ m/s

Figure 10

Figure 9: Figure 10

(a) Velocity contour map of the $Y = 0.5$ m section

(b) Velocity vector map of the $Z = 0$ m section

Fig. 10 Velocity contour of $Y = 0.5$ m section and velocity vector image of $Z = 0$ m section under three placement modes when $V = 0.3$ m/s

Figure 11

Figure 10: Figure 11

(a) Velocity contour map of the $Y = 0.5$ m section

(b) Velocity vector map of the $Z = 0$ m section

Fig. 11 Velocity contour of $Y = 0.5$ m section and velocity vector image of $Z = 0$ m section under three placement modes when $V = 0.5$ m/s

The upwelling and back-eddy volume indices were selected to quantitatively analyze the hydrodynamic characteristics of the reef under different layout schemes. For the upwelling region, the vertical velocity was taken as greater than 5% of the incoming velocity, whereas for the back-eddy region it was taken as less than 80% of the incoming velocity

16

. Figures 12(a) and 12(b) show the shapes of the upwelling and back-eddy regions, respectively, when the reef is placed perpendicular to the mainstream direction at an incoming velocity of 0.1 m/s.

Fig. 12 Upwelling and back eddy area

Figure 11: Fig. 12 Upwelling and back eddy area

(a) Upwelling (b) Back eddy

Fig. 12 Upwelling and back eddy area

The volumes of the upwelling and back-eddy regions obtained by integration for each calculation scheme are shown in Fig. 13.

Fig. 13 Volume size of upwelling and back eddy in different calculation schemes

It can be seen from Fig. 13 that, under different angles of attack and incoming-flow velocities, the volumes of the reef' s upwelling and back-eddy regions vary

Fig. 13 Volume size of upwelling and back eddy in different calculation schemes

Figure 12: Fig. 13 Volume size of upwelling and back eddy in different calculation schemes

considerably, and both the upwelling and back-eddy volumes increase with increasing flow velocity. When the incoming velocity is 0.1 m/s, because the flow velocity is relatively low, the volumes of upwelling and back eddy generated when the reef is placed perpendicular to the mainstream direction are slightly larger than those corresponding to placement at an angle of 45° to the mainstream direction. When the incoming velocity is 0.5 m/s, the upwelling and back-eddy volumes generated at an angle of attack of 45° are both the largest, with maxima of 173.26 m^3 and 133.63 m^3, respectively; at this time, the reef has a better flow-field effect. Therefore, considering comprehensively that a higher flow-field benefit can be obtained, when deploying artificial reefs, the reef body may be arranged at an angle of 45° to the mainstream direction of the ocean current, thereby forming relatively large upwelling and back-eddy regions.

3.2 Effect of placement spacing

The spacing arrangement between reefs has a certain influence on the flow-field effect of artificial reefs

34

. Transverse spacings of 1.0, 1.5, 2.0, and 2.5 L were selected, and longitudinal spacings of 1.0, 1.5, 2.0, and 2.5 L were selected. The incoming velocity was set to 0.5 m/s, and each reef was placed at an angle of 45° to the incoming-flow direction.

Figure 14 shows velocity contours on the horizontal section $Y = 0.5$ m when two reefs are arranged transversely with different spacings. As the spacing increases, the mutual influence of the flow fields around the two reefs gradually weakens; the area of the deceleration region in front of the reefs gradually increases and, at a spacing of $2L$, splits into two regions. The wake region behind the reefs gradually separates from two parts into multiple regions; the total affected area increases and also becomes more dispersed. The high-speed region between the two reefs also increases with increasing spacing, causing the relatively large back-eddy regions behind the two reefs to gradually separate.

Fig. 14 Velocity contour of two reefs placed horizontally on a section of Y = 0.5 m

Figure 13: Fig. 14 Velocity contour of two reefs placed horizontally on a section of Y = 0.5 m

(a) Spacing $1L$ (b) Spacing $1.5L$

(b) Spacing $2L$ (d) Spacing $2.5L$

Fig. 14 Velocity contour of two reefs placed horizontally on a section of $Y = 0.5$ m

Fig. 15 shows velocity contour maps on the horizontal section of $Y = 0.5$ m under different spacings when two reefs are arranged longitudinally. As the spacing increases, the flow field in the slow-flow region in front of the reefs shows no obvious change, while the wake flow generated by the two reefs is continuously broken up and diffused by the velocity contours of the flow field, making the complexity of the flow field behind the reefs continuously increase.

Fig. 15

Figure 14: Fig. 15

(a) Spacing $1L$

(b) Spacing $1.5L$

(c) Spacing $2L$

(d) Spacing $2.5L$

Fig. 15 Velocity contour of two reefs placed longitudinally on a section of $Y = 0.5$ m

Fig. 16 presents the flow-field effect results for two reefs placed horizontally and longitudinally at different spacings. When the horizontal spacing is $1.5L$, while satisfying the requirement for a relatively large volume of upwelling, it also produces the maximum volume of back-eddy flow; moreover, the upwelling and back-eddy flow regions are connected into one continuous area, which is beneficial to the aggregation of marine organisms. As the longitudinal spacing between the two reefs increases, the volumes of the generated upwelling and back-eddy flow both increase continuously, reaching their maxima at a spacing of $2.5L$, namely 295.26 m^3 and 231.88 m^3, respectively. Therefore, when two reefs are placed with a horizontal spacing of $1.5L$ and a longitudinal spacing of $2.5L$, they exhibit comprehensively superior upwelling and back-eddy flow effects in the flow field.

Fig. 16

Figure 15: Fig. 16

(a) Horizontal placement

(b) Longitudinal placement

Fig. 16 Comparison of flow effects between horizontal placement and longitudinal placement

3.3 Influence of reef-group layout schemes

In marine ranches, artificial reefs are often arranged according to reef-group planning, and the relationship between the layout mode and the flow-field effect becomes more complex. In this study, a reef group consisting of 30 artificial reefs was considered, and four schemes were formulated for comparative study. The reefs were evenly divided into 6 rows, with each row arranged either in a straight line with front–back alignment or in a straight line with staggered placement, and in an arc with front–back alignment or in an arc with staggered placement. The arrangement spacing of the reefs in each row was horizontal 3 m ($1.5L$) and longitudinal 5 m ($2.5L$). The incoming-flow velocity was set to 0.5 m/s, and each reef was placed at an angle of 45° to the incoming-flow direction. Fig. 17 shows the velocity contour maps of the flow fields for the four schemes. When arranged in a staggered pattern, the wake flow field of the reef group undergoes a larger-amplitude deflection. At a horizontal spacing of 3 m, a large, contiguous deceleration region forms in front of the reef group. The shape of the velocity contours in front of the reef group changes with arc arrangement and linear arrangement, representing the portion with relatively large changes in the flow-field morphology. A large number of low-velocity vortices exist in the middle region of the reef group, and the overall wake flow field formed is complex.

The differences in the wake-flow-field morphology are not large.

Table 2 gives the volumes of the upwelling and back-eddy regions under different layouts of 30 reefs. Compared with the circular-arc arrangement, the linear arrangement has larger upwelling and back-eddy volumes; compared with the aligned arrangement, the staggered arrangement has larger upwelling and back-eddy volumes. Overall, reef groups arranged in a linear staggered pattern have a greater influence on the flow field behind the reef body and produce better flow-field effects, but the advantage is not significant.

Fig. 17 Velocity contour of 30 reefs with different arrangements on a section of Y = 0.5 m

Figure 16: Fig. 17 Velocity contour of 30 reefs with different arrangements on a section of Y = 0.5 m

(a) Linear aligned layout

(b) Linear staggered layout

(c) Circular-arc aligned layout

(d) Circular-arc staggered layout

Fig. 17 Velocity contour of 30 reefs with different arrangements on a section of $Y = 0.5$ m

Table 2 Volume of upwelling and back eddy of 30 reefs with different layouts

Layout mode	Upwelling-region volume /m^3	Back-eddy-region volume /m^3
$V = 0.5$ m/s linear staggered layout	3 075.59	1 590.14
$V = 0.5$ m/s circular-arc staggered layout	3 030.88	1 517.98
$V = 0.5$ m/s linear aligned layout	3 002.45	1 518.69
$V = 0.5$ m/s circular-arc aligned layout	2 917.95	1 494.16

4 Conclusions

To study the effects of the incident-flow angle, reef-group arrangement spacing, and arrangement mode on the flow-field effects when rectangular frame-type artificial reefs are deployed, the flow velocities at representative positions around a rectangular frame-type artificial reef model were measured, the typical flow-field characteristics around the reef model were further measured by PIV, and the effects of different incoming-flow velocities, incident-flow directions, and arrangement modes on the flow-field effects of rectangular frame-type artificial reefs were analyzed by numerical simulation. The following main conclusions were obtained.

1) At an incoming-flow velocity of 0.1 m/s, artificial reefs arranged perpendicular to the mainstream direction produce larger upwelling and back-eddy volumes in the flow field. At incoming-flow velocities of 0.3 m/s and 0.5 m/s, artificial reefs arranged at an oblique angle of 45° to the mainstream direction have larger upwelling and back-eddy volumes and produce a relatively more complex wake region. Under the same incident-flow angle, the upwelling volume and back-eddy volume increase with increasing incoming-flow velocity.

2) At an incoming-flow velocity of 0.5 m/s, when two reefs are placed longitudinally, the upwelling and back-eddy volumes increase as the spacing increases. When two reefs are placed transversely, the upwelling volume changes little when the spacing is $1.5L$–$2.5L$, and the back-eddy volume reaches its maximum at a spacing of $1.5L$. When arranged with a longitudinal spacing of $2.5L$ and a transverse spacing of $1.5L$, the reefs have, overall, larger upwelling and back-eddy volumes in the flow field.

3) For a reef group composed of 30 reef units, compared with the layout in which each row of reefs is arranged along an arc, arranging them along straight lines produces larger upwelling and wake-flow regions. Overall, the reef group with a straight staggered arrangement has a greater in-

fluence on the flow field around the reefs located downstream, and its flow-field effect is better; however, the overall advantage is not significant.

References:

[1] BAINE M. Artificial reefs: a review of their design, application, management and performance[J]. *Ocean & Coastal Management*, 2001, 44(3/4): 241-259.

[2] ZHANG Shuo, ZHANG Shidong, HU Fuxiang, et al. Comparison of numerical simulation and a test model of a hexagonal and square opening artificial reef[J]. *Journal of Fishery Sciences of China*, 2020, 27(11): 1350-1359 (in Chinese).

[3] YU Dingyong, ZHAO Wei, WANG Fengyu, et al. Trapezoid artificial reefs in different deployment spacing: physical and numerical simulations[J]. *Oceanologia et Limnologia Sinica*, 2020, 51(2): 283-292 (in Chinese).

[4] LIU Yang, HUANG Guoxing. Experimental study on flow field effect of hexagonal artificial reef[J]. *China Water Transport*, 2021(11): 60-62 (in Chinese).

[5] ZHENG Yanxuan, LIANG Zhenlin, GUAN Changtao, et al. Numerical simulation and experimental study on flow field of artificial reefs in three tube-stacking layouts[J]. *Oceanologia et Limnologia Sinica*, 2014, 45(1): 11-19 (in Chinese).

[6] ZHANG Shuo, ZHANG Shidong, CHU Wenhua, et al. Model experiment of hydrodynamic performance of square artificial reefs with hexagonal openings[J]. *Journal of Fisheries of China*, 2020, 44(11): 1903-1912 (in Chinese).

[7] YE Gongzhao, WANG Ying, CHEN Shun, et al. Experimental study on hydrodynamic performance of two frame-type artificial reefs in Nanji Islands waters[J]. *Fishery Modernization*, 2021, 48(1): 25-32 (in Chinese).

[8] NISUGI K, HAYASE T, SHIRAI A. Fundamental study of hybrid wind tunnel integrating numerical simulation and experiment in analysis of flow field[J]. *JSME International Journal Series B Fluids and Thermal Engineering*, 2004, 47(3): 593-604.

[9] FANG Jihong, LIN Jun, YANG Wei, et al. Numerical simulation of flow field effect around the double-layer cross-wing artificial reef[J]. *Journal of Shanghai Ocean University*, 2021, 30(4): 743-754 (in Chinese).

[10] LIU Xinmei, ZHENG Yanna, CHEN Changping, et al. Numerical simulation of flow around frame and caisson artificial reef models[J]. *Journal of Dalian Ocean University*, 2019, 34(1): 133-138 (in Chinese).

[11] JIANG Z Y, LIANG Z L, LIU Y, et al. Particle image velocimetry and numerical simulations of the hydrodynamic characteristics of an artificial reef[J]. *Chinese Journal of Oceanology and Limnology*, 2013, 31(5): 949-956.

[12] CUI Enping, ZHANG Yongqiang, ZHU Lin, et al. Numerical simulation of the influence of artificial reefs on marine hydrodynamics to the west of Qianlian Island[J]. *Marine Geology Frontiers*, 2021, 37(2): 10-20 (in Chinese).

[13] WANG Jiahao, LIU Lili, CAI Xinchen, et al. Numerical simulation study on influence of disposal space on effects of flow field around porous square artificial reefs[J]. *Progress in Fishery Sciences*, 2020, 41(3): 40-48 (in Chinese).

[14] YU Dingyong, WANG Fengyu, ZHONG Yanchao, et al. Numerical research on hydrodynamic characteristics of artificial reefs with different disposal spaces[J]. *Periodical of Ocean University of China*, 2020, 50(2): 126-134 (in Chinese).

[15] LIU Yan, GUAN Changtao, ZHAO Yunpeng, et al. Experimental study on two-dimensional flow field of the star artificial reef in the water stream with PIV[J]. *Chinese Journal of Hydrodynamics*, 2010, 25(6): 777-783 (in Chinese).

[16] YU Congda, YU Duan, YAN Shiqiang. Hydrodynamic simulation to the best layout of artificial ship-reefs[J]. *Oceanologia et Limnologia Sinica*, 2004, 35(4): 299-305 (in Chinese).

[17] LIU Hongsheng, MA Xiang, ZHANG Shouyu, et al. Model experiment on the flow-field effect of artificial reefs[J].

Journal of Fisheries of China, 2009, 33(2): 229-236.
LIU Hongsheng, MA Xiang, ZHANG Shouyu, et al. Research on model experiments of effects of artificial reefs on flow field [J]. Journal of Fisheries of China, 2009, 33(2): 229-236 (in Chinese).

[18] LIU T L, SU D T. Numerical analysis of the influence of reef arrangements on artificial reef flow fields [J]. Ocean Engineering, 2013, 74: 81-89.

[19] LIU Y, ZHAO Y P, DONG G H, et al. A study of the flow field characteristics around star-shaped artificial reefs [J]. Journal of Fluids and Structures, 2013, 39: 27-40.

[20] LAN C H, CHEN C C, HSUI C Y. An approach to design spatial configuration of artificial reef ecosystem [J]. Ecological Engineering, 2004, 22(4/5): 217-226.

[21] LAN C H, HSUI C Y. The deployment of artificial reef ecosystem: modelling, simulation and application [J]. Simulation Modelling Practice and Theory, 2006, 14(5): 663-675.

[22] WANG G, WAN R, WANG X X, et al. Study on the influence of cut-opening ratio, cut-opening shape, and cut-opening number on the flow field of a cubic artificial reef [J]. Ocean Engineering, 2018, 162: 341-352.

[23] JIANG Z Y, LIANG Z L, TANG Y L, et al. Numerical simulation and experimental study of the hydrodynamics of a modeled reef located within a current [J]. Chinese Journal of Oceanology and Limnology, 2010, 28(2): 267-273.

[24] LI J, ZHENG Y X, GONG P H, et al. Numerical simulation and PIV experimental study of the effect of flow fields around tube artificial reefs [J]. Ocean Engineering, 2017, 134: 96-104.

[25] XIAO Rong, YANG Hong. Numerical simulation on features of flow field around hollow artificial reefs [J]. Journal of Shanghai Ocean University, 2015, 24(6): 934-942.
XIAO Rong, YANG Hong. Numerical simulation on features of flow field around hollow artificial reefs [J]. Journal of Shanghai Ocean University, 2015, 24(6): 934-942 (in Chinese).

[26] FU Dongwei, CHEN Yong, CHEN Yanshun, et al. PIV experimental study of the flow-field effects of square artificial reef monomers [J]. Journal of Dalian Ocean University, 2014, 29(1): 82-85.
FU Dongwei, CHEN Yong, CHEN Yanshun, et al. PIV experiment of artificial monomer reefs on the flowing field [J]. Journal of Dalian Ocean University, 2014, 29(1): 82-85 (in Chinese).

[27] SHAO Wanjun, LIU Changgen, NIE Hongtao, et al. Analysis of hydrodynamic characteristics and flow-field effects of artificial reefs [J]. Chinese Journal of Hydrodynamics, Series A, 2014, 29(5): 580-585.
SHAO Wanjun, LIU Changgen, NIE Hongtao, et al. Analysis of hydrodynamic characteristics and flow field around artificial reefs [J]. Chinese Journal of Hydrodynamics, 2014, 29(5): 580-585 (in Chinese).

[28] LIU Yan, ZHAO Yunpeng, CUI Yong, et al. Experimental study of the flow-field effects of cube artificial reefs [J]. Ocean Engineering, 2012, 30(4): 103-108.
LIU Yan, ZHAO Yunpeng, CUI Yong, et al. Experimental study of the flow field around cube artificial reef [J]. The Ocean Engineering, 2012, 30(4): 103-108 (in Chinese).

[29] XIAO Zhixiang. Numerical Simulation of Complex Flows with the Navier-Stokes Equations and Application of Turbulence Models [D]. Xi' an: Northwestern Polytechnical University, 2003.

[30] SMITH L M, WOODRUFF S L. Renormalization-group analysis of turbulence [J]. Annual Review of Fluid Mechanics, 1998, 30: 275-310.

[31] ZHENG Yanxuan, GUAN Changtao, SONG Xiefa, et al. Numerical simulation of the flow-field effects of star-shaped artificial reefs [J]. Transactions of the Chinese Society of Agricultural Engineering, 2012, 28(19): 185-193.
ZHENG Yanxuan, GUAN Changtao, SONG Xiefa, et al. Numerical simulation on flow field around star artificial reefs [J]. Transactions of the Chinese Society of Agricultural Engineering, 2012, 28(19): 185-193 (in Chinese).

[32] FENG Jing' an, TANG Xiaoqi, WANG Weibing, et al. Reliability verification method of numerical simulation based on grid independence and time independence [J]. Journal of Shihezi University (Natural Science), 2017, 35(1): 52-56.
FENG Jing' an, TANG Xiaoqi, WANG Weibing, et al. Reliability verification

method of numerical simulation based on grid independence and time independence [J]. Journal of Shihezi University (Natural Science), 2017, 35(1): 52-56 (in Chinese).

[33] YU Dingyong, YANG Yuanhang, LI Yujia. Research on hydrodynamic characteristics and stability of artificial reefs with different opening ratios [J]. Periodical of Ocean University of China (Natural Science), 2019, 49(4): 128-136.
YU Dingyong, YANG Yuanhang, LI Yujia. Research on hydrodynamic characteristics and stability of artificial reefs with different opening ratios [J]. Periodical of Ocean University of China, 2019, 49(4): 128-136 (in Chinese).

[34] CUI Yong, GUAN Changtao, WAN Rong, et al. Numerical simulation of the influence of deployment spacing on the flow-field effects of artificial reefs [J]. Transactions of Oceanology and Limnology, 2011(2): 59-65.
CUI Yong, GUAN Changtao, WAN Rong, et al. Numerical simulation on influence of disposal space on effects of flow field around artificial reefs [J]. Transactions of Oceanology and Limnology, 2011(2): 59-65 (in Chinese).

(Editor: Zhang Lu)

Figures

Source: ChinaXiv. Machine translation. Verify with the original.

Figure 17: Figure 1

Figure 18: Figure 2

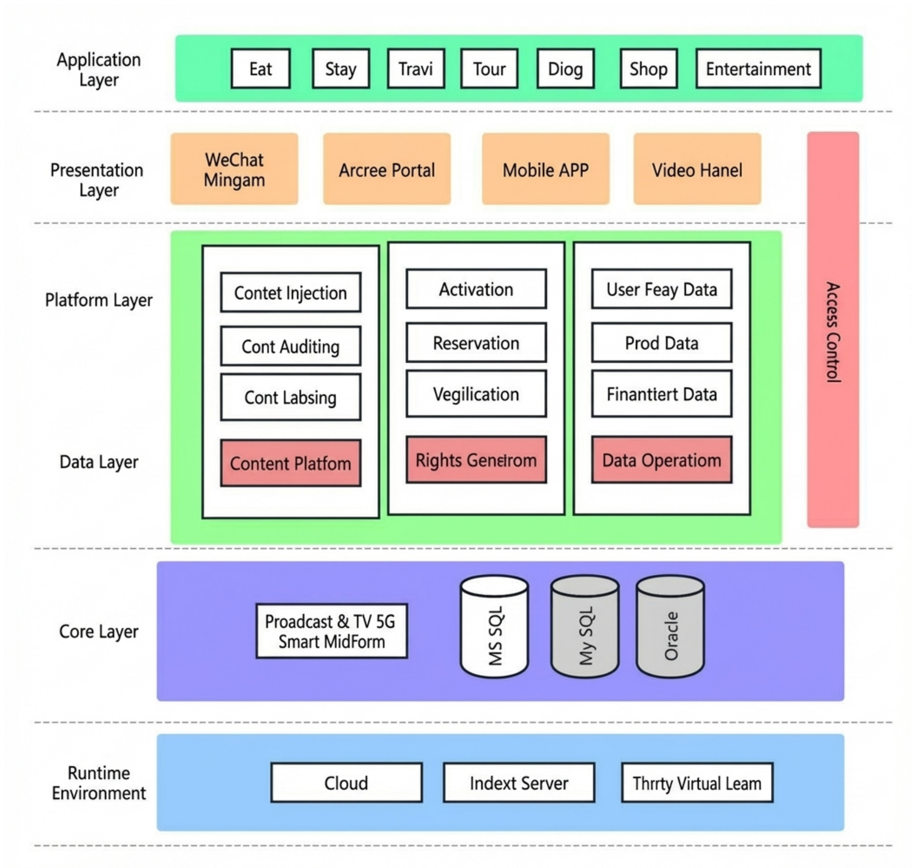

Figure 19: Figure 3

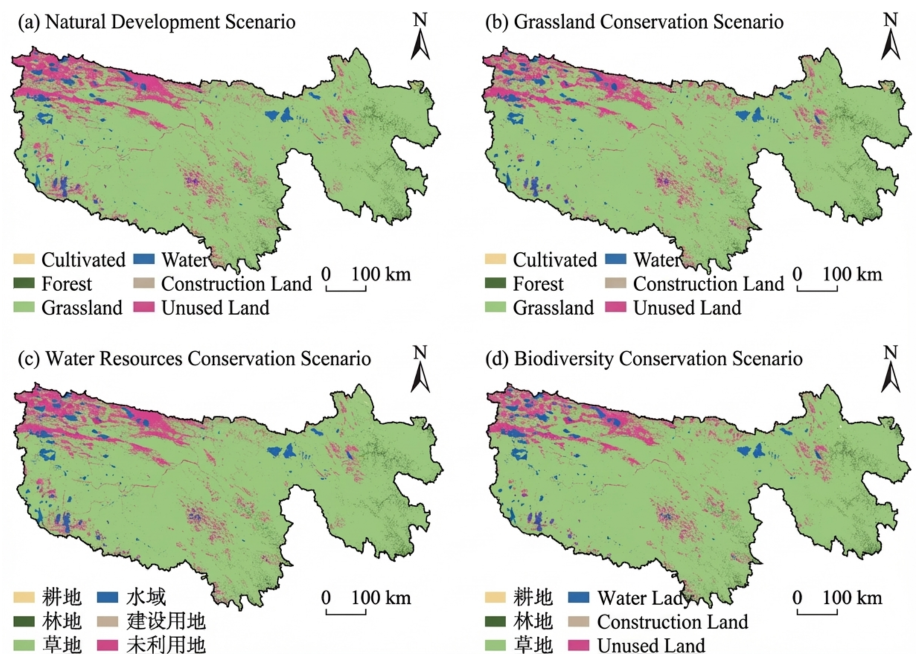

Figure 20: Figure 6

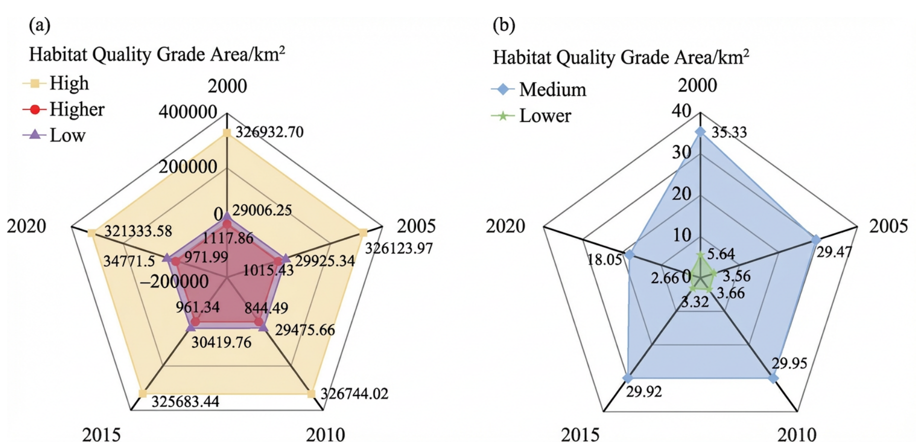

Figure 21: Figure 8

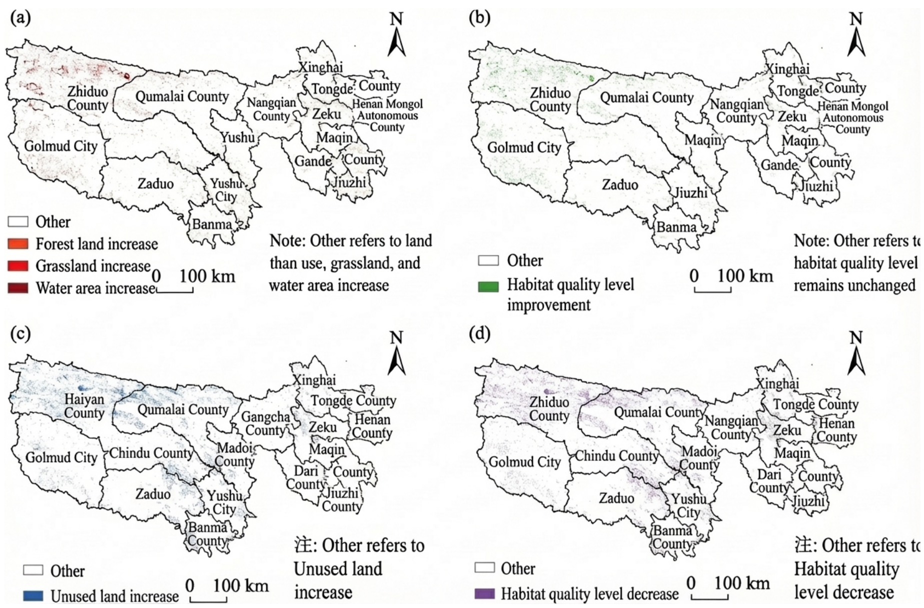

Figure 22: Figure 9

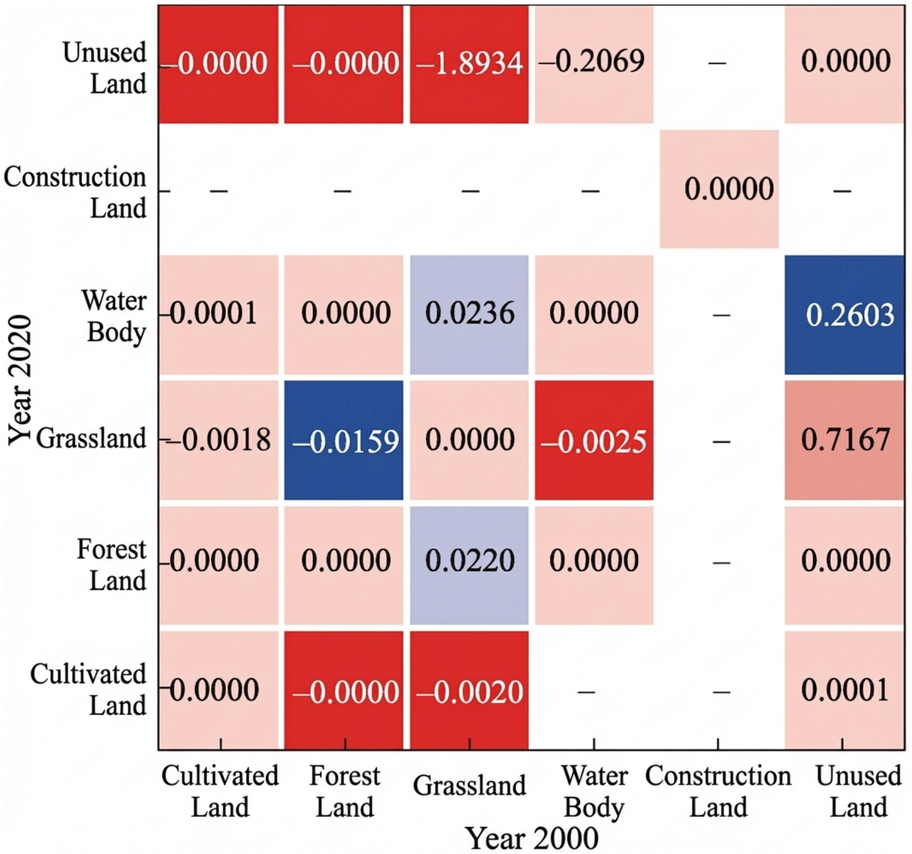

Figure 23: Figure 10

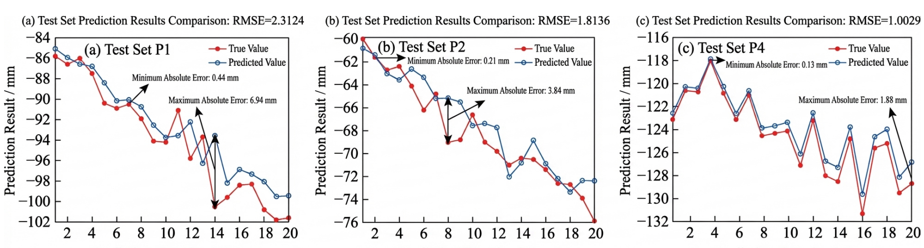

Figure 24: Figure 11